Phases, collective modes, and non-equilibrium dynamics of dissipative Rydberg atoms

S. Ray,[1] S. Sinha,[1] and K. Sengupta[2]

[1] *Indian Institute of Science Education and Research-Kolkata, Mohanpur, Nadia-741246, India*
[2] *Department of Theoretical Physics, Indian Association for the Cultivation of Science, Jadavpur, Kolkata-700032, India.*

(Dated: November 25, 2015)

We use a density matrix formalism to study the equilibrium phases and non-equilibrium dynamics of a system of dissipative Rydberg atoms in an optical lattice within mean-field theory. We provide equations for the fixed points of the density matrix evolution for atoms with infinite on-site repulsion and analyze these equations to obtain their Mott insulator- superfluid (MI-SF) phase boundary. A stability analysis around these fixed points provides us with the excitation spectrum of the atoms both in the MI and SF phases. We study the nature of the MI-SF critical point in the presence of finite dissipation of Rydberg excitations, discuss the fate of the superfluidity of the atoms in the presence of such dissipation in the weak-coupling limit using a coherent state representation of the density matrix, and extend our analysis to Rydberg atoms with finite on-site interaction via numerical solution of the density matrix equations. Finally, we vary the boson (atom) hopping parameter J and the dissipation parameter Γ according to a linear ramp protocol. We study the evolution of entropy of the system following such a ramp and show that the deviation of the entropy from its steady state value for the latter protocol exhibits power-law behavior as a function of the ramp time. We discuss experiments which can test our theory.

PACS numbers: 32.80.Ee, 03.75.Lm, 05.30.Jp, 05.30.Rt, 64.60.Ht

arXiv:1511.05157v2 [cond-mat.str-el] 24 Nov 2015

I. INTRODUCTION

In recent years the experimental and theoretical study of Rydberg atoms has become an active area of research in the field of ultracold quantum gases and condensed matter physics[1–13]. In Rydberg atoms, a valence electron may be excited to a state of large principal quantum number by suitable laser driving. The presence of large polarizibility of such excited states leads to strong Van der Walls force between these excited atoms; this force turns out to be the main ingredient for strong correlation in ultracold Rydberg system. Such strong Van der Walls interaction of a Rydberg excited atom hinders another excitation within a certain radius from it. This phenomenon, known as Rydberg (dipole) blockade, has been studied both theoretically[1] and experimentally[2]. It has been shown that the long range Van der Walls interaction between the Rydberg excited atoms leads to the formation of density ordering and translational symmetry broken phases like supersolid (SS) droplets within superfluid (SF) phase of these atoms[3]. Also an effective spin model with antiferromagnetic ordering can be realized in a system of frozen Rydberg atoms (with vanishing kinetic energy of the atoms) due to the long range interaction[4]. In a recent experiment on Rydberg atoms in an optical lattice it has been demonstrated that the superfluidity is not destroyed by the strong interaction between the excited atoms[13]. Various exotic phases and collective excitations of Rydberg gas in an optical lattice has been studied theoretically[14].

Another important property of a Rydberg atom is its finite lifetime in the excited state[15]. Due to such a finite decay rate of the excitations, ultracold Rydberg gases constitute a non-equilibrium quantum many body system. In a recent experiment an ensemble of dilute thermal Rydberg gas has been shown to undergo a non-equilibrium phase transition between states of high and low Rydberg occupancy which is induced by resonant dipolar interaction between the atoms[16]. Such a transition is marked by critical slowing down which can be detected by measurement of time taken by the system to reach the steady after being optically excited by an external laser source[16]. This phenomenon has been theoretically analyzed by modeling the frozen Rydberg atoms as a dissipative spin system with decay and dephasing[17]. Such an analysis revealed the existence of a non-conserved order parameter with a definite Z_2 symmetry which attains finite values as the system moves across the non-equilibrium transition to the large dipolar interaction regime. Further, such frozen Rydberg atoms, in the presence of a bipartite lattice and in the zero hopping limit, was shown to undergo a quantum phase transition from an uniform to a translational symmetry broken (antiferromagnetic) state[18]; the details of the transition has been analyzed using density matrix formulation within mean-field theory which indicated the existence of non-equilibrium steady states in these systems[18]. Various other non-equilibrium properties of frozen Rydberg gases and their relaxation dynamics have been studied theoretically[19,20]. However the fate of the superfluid phase and the Mott-superfluid transition of these atoms remains beyond the scope of the models used in these studies since the frozen limit of the Rydberg atoms is analogous to setting their hopping strength J to zero in a lattice. Thus the effect of finite lifetime of the Rydberg excitations on the superfluid order parameter and the Mott insulator-superfluid (MI-SF) transition of such systems has not been studied so far. However, recent experiments has led to realization of Bose-condensate of Rydberg atoms[13]. The interpretation of such exper-

imental results and its analog in the strong coupling regime clearly necessitates a formalism for treating Rydberg atoms in the presence of a finite excitation lifetime beyond the frozen limit; to the best of knowledge such a formalism has not been developed so far and we aim to fill up this gap in the present work.

In this work, we analyze the Rydberg atoms using a density matrix formalism and within mean-field theory. We chart out the possible homogeneous steady states of Rydberg atoms in an optical lattice in the strong coupling regime with a finite hopping strength J and allowing for a finite decay time for Rydberg excitations characterized by a decay rate Γ, as a function of J and Γ. We analyze the time evolution of the Rydberg bosons and obtain the possible steady states of the system from the fixed points of the density matrix evolution equations. Our analysis of the fixed point equations, in the limit of infinite on-site boson repulsion (hardcore limit), leads to determination of the MI-SF phase boundary of these atoms as a function of J and Γ. We also carry out a stability analysis around these fixed points to chart out the collective modes of the atoms in each of the phases. We supplement our analytical results with numerical studies for bosons with finite on-site repulsion and show that the phase diagram so obtained is qualitatively similar to that for atoms with infinite on-site repulsion for a wide range of chemical potential. Next, we use a coherent state representation of the boson density matrix deep in the SF phase in the weak-coupling limit and obtain their collective modes; in particular, we chart out the variation of the group velocity of the bosons with Γ. Finally, we study non-equilibrium dynamics of these bosons subjected to a linear ramp across the transition point and discuss entropy production which accompanies such ramps. We point out that the entropy of the atoms during such ramp dynamics shows qualitatively distinct behavior depending on whether J or Γ is tuned to cross the MI-SF phase boundary. We discuss experiments that may test our theory. We note that our work, being carried out using a mean-field formalism, is expected to be qualitatively accurate for two- and three-dimensional Rydberg systems. In addition, to the best of our knowledge, it provides the first theoretical analysis of superfluidity, MI-SF transition, collective modes and non-equilibrium dynamics of such dissipative Rydberg atoms in the strong-coupling regime; we therefore expect this work to be of interest to both experimentalists and theorists working on this system.

The plan of the rest of the work is as follows. In Sec. II, we formulate the evolution equation for the density matrix, obtain analytical expressions of the MI and SF fixed points from it in the infinite on-site repulsion (hard core) limit, and chart out the MI-SF phase boundary using these equations. This is followed by Sec. III, where we carry out the stability analysis around these fixed points and obtain the collective modes in each of the phases. We also carry out numerical analysis of the phases of the soft-core bosons in this section. This is followed by Sec. IV, where we use a coherent state representation of the density matrix to discuss the fate of superfluidity of the Rydberg bosons in the weak-coupling limit. Next, in Sec. V, we discuss non-equilibrium dynamics of these systems for a linear ramp protocol of the hopping strength J and the dissipation constant Γ and contrast several features of such dynamics from their dissipationless counterpart in closed quantum systems. Finally, we summarize our results, discuss possible experiments relevant to our theory, and conclude in Sec. VI.

II. PHASES OF HARDCORE BOSON

The Hamiltonian of the Rydberg atoms in the presence of an optical lattice are described by $H = H_0 + H_1 + H_2$ with

$$H_0 = \Omega \sum_i (a_i^\dagger b_i + h.c.) - \mu_0 \sum_i \hat{n}_i + \Delta \sum_i n_i^b + \frac{U}{2} \sum_i \hat{n}_i^a (\hat{n}_i^a - 1) + \lambda_0 U \sum_i \hat{n}_i^a \hat{n}_i^b \quad (1)$$

$$H_1 = -\frac{J}{2} \sum_{\langle ij \rangle} (a_i^\dagger a_j + \eta b_i^\dagger b_j + h.c.) \quad (2)$$

$$H_2 = \frac{V_d}{2} \sum_{ij} \frac{\hat{n}_i^b \hat{n}_j^b}{|r_i - r_j|^6} \quad (3)$$

where $a_i(b_i)$ are annihilation operator for boson at site i in the ground(excited) state, $\hat{n}_i^{a(b)} = a_i^\dagger a_i (b_i^\dagger b_i)$ are the corresponding number operators with $\hat{n}_i = \hat{n}_i^a + \hat{n}_i^b$, V_d is the interaction strength between neighboring bosons in the excited states, J(ηJ) is the hopping strength of ground(excited) state bosons, μ_0 is the chemical potential, $U(\lambda_0 U)$ are the on-site interaction strength between two bosons in ground (different) states, Ω is the effective Rabi coupling between Rydberg bosons in the ground and the excited state, and Δ is the on-site energy cost for producing a Rydberg excitation which can be tuned to be negative in experimental systems. In the rest of this work we shall set $\hbar = 1$ and measure all energy (time) in units of $\Omega(1/\Omega)$ unless stated otherwise. The dynamics of the system's density matrix $\hat{\rho}$ is governed by

$$\frac{\partial \hat{\rho}_i}{\partial t} = -i \left[\hat{H}_i^{MF}, \hat{\rho}_i \right] + \hat{\mathcal{L}} \hat{\rho}$$
$$\hat{\mathcal{L}} \hat{\rho} = \sum_j (\hat{L}_{ij} \hat{\rho}_i \hat{L}_{ij}^\dagger - \frac{1}{2} \hat{L}_{ij}^\dagger \hat{L}_{ij} \hat{\rho}_i - \frac{1}{2} \hat{\rho}_i \hat{L}_{ij}^\dagger \hat{L}_{ij}) \quad (4)$$

where $L = \sqrt{\Gamma} a^\dagger b$ represents the decay of an Rydberg atom from the excited to the ground state. In this section, we shall study these equations for hardcore bosons for which $U \to \infty$. For such bosons, the states of the systems can be expressed in the basis $|n_a, n_b\rangle$; at each site the boson states are linear combination of $|0,0\rangle$, $|1,0\rangle$ and $|0,1\rangle$. Further within mean-field theory and as long as we restrict ourselves to the study of the homogeneous

phases of the system, the Hamiltonian of the system can be written as $H_{\rm mf} = \sum_i H_i$ where H_i is given by

$$H_i = \begin{pmatrix} 0 & -\frac{Jz}{2}\langle a_j^\dagger\rangle & -\frac{\eta Jz}{2}\langle b_j^\dagger\rangle \\ \frac{-Jz}{2}\langle a_j\rangle & -\mu_0 & 1 \\ -\frac{\eta Jz}{2}\langle b_j\rangle & 1 & -\mu_0 + \Delta + \frac{Vz}{2}\langle n_{2j}\rangle \end{pmatrix} \quad (5)$$

where j denote any one of the nearest-neighbor sites of i and z is the coordination number of the lattice. We note here that for homogeneous phases $\langle O_j\rangle \equiv \langle O\rangle$ for any operator O. Also, all energies in Eq. 5 are dimensionless quantities scaled in units of Ω; for example $J \equiv J/\Omega$. The density matrix can be written using the above-mentioned basis, as

$$\hat{\rho}_i = \begin{pmatrix} n_0 & \alpha & \beta \\ \alpha^* & n_1 & \gamma \\ \beta^* & \gamma^* & n_2 \end{pmatrix} \quad (6)$$

where $\alpha = \langle a^\dagger\rangle$ and $\beta = \langle b^\dagger\rangle$ are the order parameters for ground and excited states state superfluidity, $\gamma = \langle a^\dagger b\rangle$, $n_i = \langle \hat{n}_i\rangle$ for $i = 1, 2$ are the boson number density for ground and excited states, and $n_0 = \langle |0,0\rangle\langle 0,0|\rangle$. Here the average of the operators are represented by $\langle . \rangle = {\rm Tr}[.\hat{\rho}_i]$. Using Eqs. 4, 5 and 6, we get the following dynamical equations

$$\dot{n}_0 = 0 \quad \dot{n}_{1(2)} = -(+)i(\gamma^* - \gamma) + (-)\Gamma n_2 \quad (7a)$$

$$\dot{\alpha} = i\left[(zJ(n_1 - n_0)/2 - \mu_0)\alpha + (\eta zJ\gamma^*/2 + 1)\beta\right] \quad (7b)$$

$$\dot{\beta} = i\left[(zJ\gamma/2 + 1)\alpha + (\eta zJ(n_2 - n_0)/2 - \mu_0 + \Delta + zVn_2/2)\beta\right] - \Gamma\beta/2 \quad (7c)$$

$$\dot{\gamma} = i\left[Jz\alpha^*\beta(1-\eta)/2 - (n_2 - n_1) + (\Delta + zVn_2/2)\gamma\right] - \Gamma\gamma/2 \quad (7d)$$

where dot represents the derivative with respect to scaled time $t \equiv t\Omega$. From the single site mean field dynamical equations we see that n_0 is a free parameter which remains constant with time. As a result, the density of the system remains constant in the dynamics and is given by $\langle \hat{n}\rangle = 1 - n_0$ due to the constraint $n_0 + n_1 + n_2 = 1$. For the time evolution of the density matrix the initial conditions to be supplied for solution of Eq. 7. To analyze the long time dynamics and steady states numerically, we are going to choose the initial density matrix as a pure state constructed from the ground state of the Gutzwiller wavefunction for $H_{\rm mf}$, since it represents the physical steady state with vanishing entropy for $\Gamma = 0$. Also this choice of initial density matrix is most natural in an experimental setup. In what follows, we first look into the fixed point structure of Eq. 7. We find that there are two distinct fixed points; the first corresponds to the MI phase and has $|\alpha| = |\beta| = 0$ while the second corresponds to the SF phase with non-vanishing α and β.

MI phase: For the Mott fixed point, γ_R and n_2 can be obtained from Eqs. 7a and 7d after setting $|\alpha| = |\beta| = 0$ in Eqs. 7b and 7c. Such a procedure yields

$$\gamma_R = -\tilde{V}n_2, \quad \gamma_I = \tilde{\Gamma}n_2 \quad (8)$$

$$(n_0 + 2n_2 - 1) + \tilde{V}^2 n_2 + \tilde{\Gamma}^2 n_2 = 0, \quad (9)$$

where $\tilde{V} = (2\Delta + Vzn_2)/2$ and $\tilde{\Gamma} = \Gamma/2$. We note from the expression of $\tilde{V}$ that Eq. 9 constitutes a cubic equation for n_2. From Eq. 8 and 9, we find that there are two distinct MI phases. The first corresponds to $n_2 = 0$ and $n_0 = 1$ which is the boson vacuum; such a MI phase occurs for large negative μ_0. In this case, there is no time evolution and $\dot{\rho} = 0$ for all t. The second corresponds to $n_2, n_1 \neq 0$ and $\gamma \neq 0$ as determined by Eqs. 8 and 9; this constitutes a MI phase with finite boson density. We concentrate on the latter phase for the rest of this work.

SF phase: Next, we look for the fixed point with nonzero $\alpha = |\alpha|\exp(i\theta_1)$ and $\beta = |\beta|\exp(i\theta_2)$ which corresponds to the steady state in the SF phase. We note at the outset that while $|\alpha|$ and $|\beta|$ assumes constant values in the steady state, α and β need not be constant since the global phase of the order parameter may fluctuate. The relative phase $\theta_r = \theta_2 - \theta_1$ of these superfluid order parameters also attain a constant value in the steady state. To find the fixed point values of α and β, it is therefore convenient to rewrite Eq. 7 as

$$|\dot{\alpha}| = \eta zJ|\beta|(\gamma_I\cos\theta_r - \gamma_R\sin\theta_r)/2 - |\beta|\sin\theta_r \quad (10a)$$

$$|\dot{\beta}| = zJ\left(\gamma_R\sin\theta_r - \gamma_I\cos\theta_r\right)|\alpha|/2 + |\alpha|\sin\theta_r - \tilde{\Gamma}|\beta| \quad (10b)$$

$$\dot{\theta}_r = \frac{Jz}{2}\Big[\eta n_2 - n_1 + (1-\eta)n_0 + (|\alpha|^2 - \eta|\beta|^2) \times(\gamma_R\cos\theta_r + \gamma_I\sin\theta_r)/(|\alpha||\beta|)\Big] + (|\alpha|^2 - |\beta|^2)\cos\theta_r/(|\alpha||\beta|) + \tilde{V} \quad (10c)$$

Since we look for time independent solutions for $|\alpha|$ and $|\beta|$, we set $|\dot{\alpha}| = |\dot{\beta}| = 0$. For the SF phase, defining $r = |\alpha|/|\beta|$, we find from Eqs. 10a and 10b

$$\tan\theta_r = \frac{\eta\tilde{J}\gamma_I}{1 + \eta\tilde{J}\gamma_R} \quad r = \frac{\tilde{\Gamma}\sec\theta_r}{\tan\theta_r - \tilde{J}(\gamma_I - \gamma_R\tan\theta_r)} \quad (11)$$

where $\tilde{J} = Jz/2$. Moreover, since $\dot{\theta}_r = 0$ using Eq. 10c, we obtain

$$\tilde{J}(1 - 2n_0 - n_2)\sec\theta_r + \left(r^{-1} - r\right) + \tilde{J}(\gamma_R + \gamma_I\tan\theta_r) \times\left(\eta r^{-1} - r\right) - (\eta\tilde{J}(n_2 - n_0) + \tilde{V})\sec\theta_r = 0 \quad (12)$$

Finally setting $\dot{\gamma} = 0$ in Eq. 7d we obtain the steady state values of γ_R and γ_I to be

$$\tilde{J}(1-\eta)|\alpha||\beta|\sin\theta_r + \tilde{V}\gamma_I + \tilde{\Gamma}\gamma_R = 0 \quad (13)$$

$$\tilde{J}(1-\eta)|\alpha||\beta|\cos\theta_r - (n_0 + 2n_2 - 1) + \tilde{V}\gamma_R - \tilde{\Gamma}\gamma_I = 0$$

We note that in the SF phase the fixed point equations assume a particularly simple for $\eta = 0$ leading to

$$\theta_r = n\pi, \quad r = 1/(\tilde{J}n_2), \quad \gamma_R = -\tilde{V}n_2$$

$$\tilde{J}^2 n_2|\alpha|^2 + (2n_2 + n_0 - 1) + \tilde{V}^2 n_2 + \tilde{\Gamma}^2 n_2 = 0 \quad (14)$$

Further, in this limit, Eq. 12 can also be simplified to obtain a solution for n_2 which is given by

$$n_2 = \left[4z(J+V)\right]^{-1}\left[(1-2n_0)Jz - 4\Delta + \sqrt{((1-2n_0)Jz - 4\Delta)^2 + 32(1 + V/J)}\right] \quad (15)$$

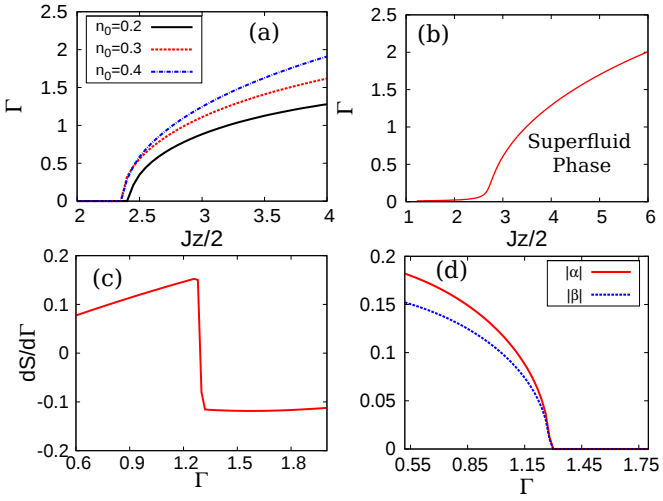

FIG. 1. Mean field phase diagram for the MI-SF transition of the Rydberg atom in the hardcore boson limit. (a) The phase boundary for different density $1-n_0$ with $\eta = 0$, $zV = 2$, and $\mu = \Delta = 0$. (b) Phase boundary for finite $\eta = 0.2$; all other parameters are same as (a). (c) Plot of the entropy derivative $dS/d\Gamma$ as a function of Γ for $zJ = 8$; all other parameters are same as in (b). (d) Plot of the order parameter amplitudes $|\alpha|$ and $|\beta|$ as a function of Γ; all parameters are same in (c). Note that $dS/d\Gamma$ shows a jump and the order parameter amplitudes vanish at the phase boundary.

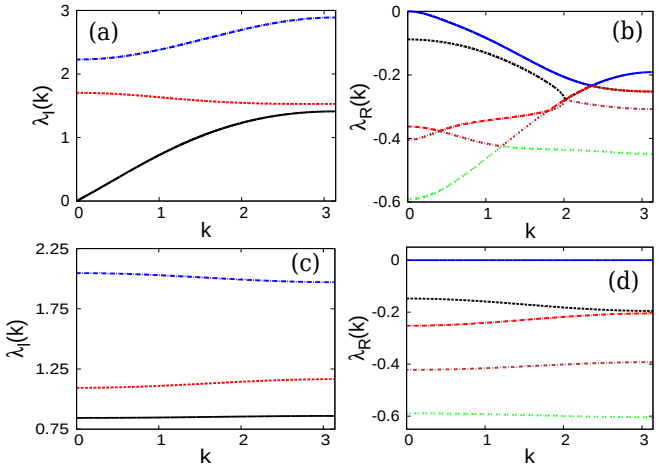

FIG. 2. Plot indicating the stability of the fixed point and corresponding to the collective models for the SF and MI phases. (a) Plot of $\lambda_I(k)$ as a function k (along a diagonal cut in the Brillouin zone) for the SF phase showing gapless and gapped excitations. The parameters used are for $zJ = 8$, $\Gamma = 0.8$, $\eta = 0.2$, $\Delta = \mu = 0$, and $zV = 2$. (b) Plot of λ_R as a function of k showing stability of the SF phase. All parameters are same as in (a). (c)-(d): Similar plots as in (a) and (b) respectively corresponding to the MI phase for $zJ = 1$; all other parameters are same as in (a). Note the absence of gapless collective modes in the MI phase.

Eqs. 7..15 constitute the complete structure of fixed points of the system both for the MI and SF phases. It turns out that only one of the two fixed points obtained is stable; their change of stability occurs at the phase transition between the MI and the SF phases. This stability analysis, which provides us information regarding the phase diagram of the system, is carried out in details in the next section. However, we note that there is an alternative way of obtaining the phase diagram from the fixed point equations. For this, one solves Eqs. 8 and 9 to get values of n_2, γ_R and γ_I; these are then substituted in Eqs. 11 and 12. A numerical solution of Eqs. 11 and 12 with these substituted values of n_2, γ_R and γ_I yields a relation between J and Γ. Since this relation holds, by construction, for both the MI and SF phases, it represents the MI-SF phase boundary. The SF phase is stabilized for $\Gamma(J)$ lower(higher) than their respective values on the phase boundary; the opposite holds for the MI phase. We note that the phase diagram obtained in this manner coincides with that obtained via stability analysis of the fixed points outlined in the next section.

The MI-SF phase diagram obtained in this manner is shown in Fig. 1(a) for several representative values of n_0 for $\eta = 0$. A similar diagram, obtained using numerical solution of Eqs. 11 and 12, is shown for $\eta = 0.2$. The order of this transition can be obtained by computing the entropy $S = -\mathrm{Tr}(\rho \log \rho)$ and $dS/d\Gamma$ across the transition. We find, as shown in Fig. 1(c), $dS/d\Gamma$ shows a jump at the phase boundary; this, together with the fact that S varies smoothly across the MI-SF boundary displaying a peak at the transition point, indicates that the transition is second order. The vanishing of the superfluid order parameter amplitudes α and β across the transition is shown in Fig. 1(d). Thus our fixed point analysis provides the complete phase diagram for the MI-SF transition.

III. STABILITY ANALYSIS AND COLLECTIVE MODES

In this section, we carry out a stability analysis of the fixed points which also enables us to obtain the dispersion of the low-energy excitations in the MI and SF phases. This is done, following standard prescription, as follows. For all of the elements of the density matrix, we study small fluctuations about the steady state values: $\rho^{ab} = \rho^{ab;(0)} + \delta\rho_i^{ab}$, where $\rho^{ab;(0)}$ is the steady state value of ρ^{ab} (Eq. 6), $\delta\rho_i^{ab}$ denotes fluctuations around the steady state value, i is the site index, and the indices a and b take values from 1 to 3. We note that $\rho^{12} \equiv \alpha$ and $\rho^{13} \equiv \beta$ shows oscillatory behavior at the fixed point whereas $|\alpha|$ and $|\beta|$ take fixed values; this allows us to parameterize $\alpha = \alpha_1 \exp(iE_f t)$ and $\beta = \beta_1 \exp(iE_f t)$ where E_f is the frequency of the oscillation. Also we note that $\delta\rho_i^{12}$ and $\delta\rho_i^{13}$ denote fluctuations corresponding to α_1 and β_1.

We substitute this form of ρ_{ij} in Eq. 7 and seek a solution of the form $\delta\rho_i^{ab}(t) = \exp(\lambda t) \sum_{\vec{k}} \exp(i\vec{k}.\vec{R}_i)\delta\rho_{\vec{k}}^{ab}$

retaining terms which are linear order in $\delta\rho^{ab}_{\vec{k}}$. We also note that since phases θ_α and θ_β of the SF order parameters α and β respectively remain undetermined up to a global phase, we choose the steady state value of β to be $\beta_1 = \alpha^*\beta/|\alpha|$ so as to have a specific relative phase, where $\alpha_1 = |\alpha|\exp[i\theta_\alpha]$ is the steady state value of α. This leads us to

$$\lambda\delta n_{1\vec{k}} = -i\Big[(\delta\gamma^*_{\vec{k}} - \delta\gamma_{\vec{k}}) - J(\alpha_1^*\delta\alpha_{\vec{k}} - \alpha_1\delta\alpha^*_{\vec{k}}) \times(z-\epsilon(\vec{k}))/2\Big] + \Gamma\delta n_{2\vec{k}} \quad (16)$$

$$\lambda\delta n_{2\vec{k}} = i\Big[(\delta\gamma^*_{\vec{k}} - \delta\gamma_{\vec{k}}) + \eta J(\beta_1^*\delta\beta_{\vec{k}} - \beta_1\delta\beta^*_{\vec{k}}) \times(z-\epsilon(\vec{k}))/2\Big] - \Gamma\delta n_{2\vec{k}} \quad (17)$$

$$\lambda\delta\alpha_{\vec{k}} = i\Big[zJ\alpha_1(\delta n_{1\vec{k}} + \delta n_{2\vec{k}}/2) + \Big(J(2n_1+n_2-1)\epsilon(\vec{k}) -2\mu - 2E_f\Big)\delta\alpha_{\vec{k}}/2 + (1+\eta\epsilon(\vec{k})J\gamma^*/2)\delta\beta_{\vec{k}} +\eta zJ\beta_1\delta\gamma^*_{\vec{k}}/2\Big] \quad (18)$$

$$\lambda\delta\beta_{\vec{k}} = i\Big[zJ\alpha_1\delta\gamma_{\vec{k}}/2 + (1+J\gamma\epsilon(\vec{k})/2)\delta\alpha_{\vec{k}} -(\mu + E_f + \eta J(1-2n_2-n_1)\epsilon(\vec{k})/2 -(\Delta + zVn_2/2))\delta\beta_{\vec{k}} + V\beta_1\epsilon(\vec{k})\delta n_{2\vec{k}}/2 +\eta zJ\beta_1(\delta n_{2\vec{k}} + \delta n_{1\vec{k}}/2)\Big] - \Gamma\delta\beta_{\vec{k}}/2 \quad (19)$$

$$\lambda\delta\gamma_{\vec{k}} = i\Big[zJ\alpha_1^*\delta\beta_{\vec{k}}/2 + J\beta_1\epsilon(\vec{k})\delta\alpha^*_{\vec{k}}/2 - \delta n_{2\vec{k}} + \delta n_{1\vec{k}} +(zVn_2/2+\Delta)\delta\gamma_{\vec{k}} + V\gamma\epsilon(\vec{k})\delta n_{2\vec{k}}/2 -\eta J\epsilon(\vec{k})\alpha_1^*\delta\beta_{\vec{k}}/2 - \eta zJ\beta_1\delta\alpha^*_{\vec{k}}/2\Big] - \Gamma\delta\gamma_{\vec{k}}/2 \quad (20)$$

where, n_1 and n_2 denote the steady state values, $\epsilon(k) = 2\sum_{i=1..d}\cos(k_i)$ where d is the dimension of the system, $\delta\alpha_{\vec{k}}$ and $\delta\beta_{\vec{k}}$ are fluctuations of α_1 and β_1 respectively. These equations are supported with another three equations for $\delta\alpha^*_{\vec{k}}$, $\delta\beta^*_{\vec{k}}$ and $\delta\gamma^*_{\vec{k}}$ and the system of these eight equations are to solved along with the constraint $n_0 + n_1 + n_2 = 1$ which shall be used to eliminate δn_0. A numerical solutions of these equations then yields the eigenmodes of the system which is shown in Fig. 2.

We first check the stability of these fixed points from such an analysis by inspecting the real part of the eigenvalues λ. We find that for a given n_0 which is chosen from the Gutzwiller ground state, Max[Re[λ]], as computed around the SF fixed point, attains zero value along a curve in the $J-\Gamma$ plane as shown in Fig. 1(a) and (b). Similarly, Max[Re[λ]], as computed around the MI fixed point becomes zero along the same curve. This curve represents the phase boundary between the MI and the SF phases and coincides with that shown in Fig. 1.

Next, we concentrate on Im[λ] which yields the dispersion of the eigenvalues. In the SF phase, our analysis finds six complex eigenvalues (three pairs corresponding to the fluctuations of α_1, β_1 and γ) and two real eigenvalues corresponding to n_1 and n_2. Among the three pairs of complex eigenmodes, the imaginary part of one gives gapless sound mode (as shown in the Fig. 2(a)) along a diagonal cut in the Brillouin zone. This is in sharp contrast to the MI phase (Fig. 2(c) and (d))where the fluctuations corresponding to α_1 and β_1 get completely decoupled from n_1, n_2 and γ. In the latter sector there is one zero mode, one real eigenvalue(≤ 0) and a pair of complex eigenvalues. Also we note the presence of a gapless sound mode in the SF phase (top left panel of Fig. 2) whereas no such mode exists in the insulating phase (bottom left panel of Fig. 2). We calculate the sound velocity($v_s = \lim_{k\to 0} d\omega/dk \equiv \lim_{k\to 0} d\lambda_I/dk$) from the linear dispersion obtained in SF phase. We note that (see Fig. 3) for a fixed J, v_s decreases with increasing Γ. We also find that the dispersion becomes quadratic ($\omega \sim k^2$) at the transition point (as shown in Fig. 3a) which indicates a dynamical critical exponent $z = 2$ for the transition. Further, we find that the energy gap ΔE at $k = 0$ satisfies $\Delta E \sim (\Gamma - \Gamma_c)$ (see Fig. 3(b)) and $\Delta E \sim (J - J_c)$. Since $\Delta E \sim (J - J_c)^{z\nu}$ at the critical point, this indicates that the correlation length exponent ν has a value 1/2 which is in accordance with mean-field theory.

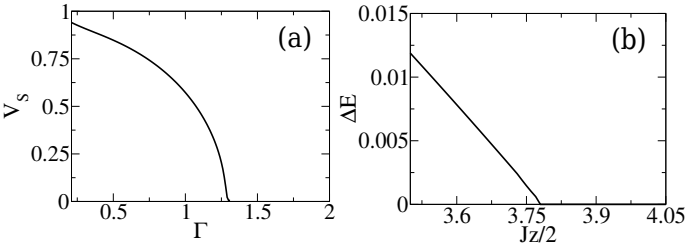

FIG. 3. (a) Plot of the superfluid velocity v_s as a function of Γ. All parameters are same as in Fig. 2(a) (b) Plot of the ΔE as a function of J for $\Gamma = 1.2$, all other parameters are same as (a).

Before ending this section, we note that an analogous analysis can be carried out numerically for soft core bosons which have finite on-site interaction U. In this case, we construct the initial density matrix of the system in the following way,

$$\hat{\rho} = |\psi\rangle\langle\psi| \quad (21)$$

where $|\psi\rangle$ is the ground state Gutzwiller wavefunction $|\psi\rangle = \Sigma_{n^a,n^b} f_{n^a,n^b}|n^a, n^b\rangle$. This wavefunction can be found out numerically by minimizing the energy functional $\langle\psi|H|\psi\rangle$. We then numerically evolve the density matrix using the Quantum Master Equation (QME) (Eq. 4) and find out the MI and SF steady states from such evolution. A stability analysis of these steady states, analogous to that described in the earlier part of this section, leads to the phase diagram for the MI-SF transition as shown in Fig. 4a. Similar to the hardcore boson, the transition line (see Fig. 4a) corresponds to the vanishing of the order parameters $\Delta_{a(b)} = \langle a(b)\rangle$. We observe near the phase boundary and for small Γ, the

relaxation time rapidly increases analogues to the critical slowing down in phase transition. Analogous to the susceptibility of the spin systems, the derivatives of the order parameters $\Delta_{a(b)}$ with respect to Γ exhibit a peak at the phase boundary which becomes sharper for longer time evolution. Finally we calculate the derivative of entropy S with respect to Γ, which is shown in Fig. 4b. A jump in the first derivative of the entropy S across the phase boundary (see Fig. 4b) indicates a continuous second order dynamical transition in the system of soft-core bosons. We note that the phase diagram obtained for bosons with finite but large U is qualitatively similar to that obtained in the $U \to \infty$ limit in Sec. II; this justifies our detailed analysis of the case of hardcore bosons where it is possible to obtain analytical results for the fixed points.

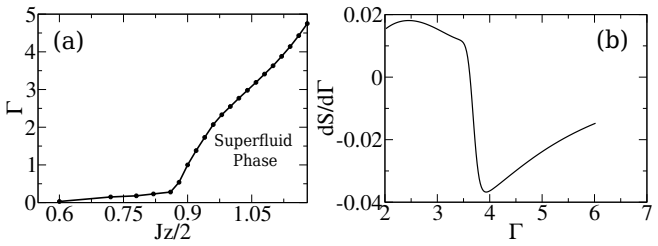

FIG. 4. (a) The MI=Sf phase boundary of soft core bosons for $U = 1.5$, $\lambda_0 = 3$, $\eta = 0.2$, $\Delta = \mu = 0$, and $zV = 2$. (b) Plot of $dS/d\Gamma$ as a function of Γ for $zJ = 2.24$; all other parameters are same as (a). Note that $dS/d\Gamma$ exhibits sharp change in slope at the critical point.

IV. DEEP SUPERFLUID LIMIT

In this section, we look into the fate of the superfluidity of the bosons in the presence of the dissipation. To this end, we adopt the coherent state description[21] of the density matrix for the bosons. We consider the coherent state

$$|\psi(t), \sigma\rangle = e^{-|\psi(t)|^2/2} e^{\psi(t) a^\dagger} |0, \sigma\rangle \tag{22}$$

where a is the annihilation operator for ground state boson, σ is the spin index where $|\uparrow\rangle(|\downarrow\rangle)$ represents 1(0) boson in the excited state, and we have used the fact that for hardcore bosons we can replace $b(b^\dagger)$ by $\sigma^-(\sigma^+)$ where $\sigma^-(\sigma^+)$ are lowering(raising) operators. The number operator in the excited state($\hat{n}_b$) can be replaced by $(1 + \hat{\sigma}_z)/2$. The mean-field single-site Hamiltonian can now be written as

$$\begin{aligned} H = & (a^\dagger \sigma^- + \sigma^+ a) - zJ(\phi_a a^\dagger + \phi_a^* a)/2 \\ & -\eta z J(\phi_b \sigma^+ + \phi_b^* \sigma^-)/2 + U \hat{n}_a(\hat{n}_a - 1)/2 \\ & +\lambda_0 U \hat{n}_a(1 + \hat{\sigma}_z)/2 + zV\langle n_{bj}\rangle(1 + \hat{\sigma}_z)/4 \\ & -\mu(\hat{n}_a + (1 + \hat{\sigma}_z)/2)) \end{aligned} \tag{23}$$

where $J(\eta J)$ are hopping strength for ground(excited) state bosons, V is the interaction strength between excited states $\phi_a = \langle a_j \rangle$, $\phi_b = \langle \sigma_j^- \rangle$ where j is the nearest neighbor index and other terms carry usual meaning. The density matrix of the system can be written in the basis of $|\psi(t), \uparrow\rangle$, $|\psi(t), \downarrow\rangle$ as,

$$\begin{aligned} \hat{\rho} = & \alpha'(t)|\psi(t), \downarrow\rangle\langle\downarrow, \psi(t)| + \beta'(t)|\psi(t), \uparrow\rangle\langle\uparrow, \psi(t)| \\ & +\gamma'(t)|\psi(t), \downarrow\rangle\langle\uparrow, \psi(t)| + \gamma'^*(t)|\psi(t), \uparrow\rangle\langle\downarrow, \psi(t)| \end{aligned} \tag{24}$$

The evolution of the density matrix of the system is given by Eq. 4 with $\hat{L} = \sqrt{\Gamma} a^\dagger \sigma^-$. Since for any operator $\hat{A}$ the time evolution is governed by

$$\frac{d\langle \hat{A} \rangle}{dt} = -i\langle [\hat{A}, \hat{H}] \rangle + \frac{1}{2}\langle [\hat{L}^\dagger, \hat{A}]\hat{L} \rangle + \frac{1}{2}\langle \hat{L}^\dagger [\hat{A}, \hat{L}] \rangle \tag{25}$$

where $\langle .. \rangle \to \mathrm{Tr}[(..)\hat{\rho}]$, we obtain the dynamical equations for ψ, γ' and β' using Eqs. 4 and 25. Here $\psi = \langle \hat{a} \rangle$, $\gamma' = \langle \hat{\sigma}^+ \rangle$ and $\beta' = \langle \hat{n}_b \rangle$ and such a procedure leads to

$$\begin{aligned} \dot{\psi}(t) = & i[zJ\phi_a/2 - U|\psi(t)|^2\psi(t) - \lambda_0 U\psi(t)\beta'(t) \\ & -\gamma'^*(t) + \mu\psi(t)] + \Gamma\psi(t)\beta'(t)/2 \end{aligned} \tag{26}$$

$$\begin{aligned} \dot{\gamma}'(t) = & i[\eta z J\phi_b^*(\beta'(t) - \alpha'(t))/2 + \lambda_0 U|\psi(t)|^2\gamma'(t) \\ & +zV\langle n_b\rangle\gamma'(t)/2 - \psi^*(t)(\beta'(t) - \alpha'(t)) - \mu\gamma'(t)] \\ & -\Gamma\gamma'(t)|\psi(t)|^2/2 \end{aligned} \tag{27}$$

$$\begin{aligned} \dot{\beta}'(t) = & i[\eta J z(\phi_b\gamma'(t) - \phi_b^*\gamma'^*(t))/2 + (\psi^*(t)\gamma'^*(t) \\ & -\psi(t)\gamma'(t))] - \Gamma\beta'(t)|\psi(t)|^2 \end{aligned} \tag{28}$$

Numerically we obtain the steady state solutions of $|\psi|$, $|\gamma'|$ and β'. We find that ψ and γ' shows oscillation with constant magnitude $|\psi|$ and $|\gamma'|$ respectively and that there is a constant relative phase between ψ and γ'. We also note from the dynamical equations that the total density of the system, $n_{\mathrm{total}} = |\psi|^2 + \beta'$ is a conserved quantity. Using this conserved quantity, we sketch a typical steady state behavior of the dynamical quantities as shown in Fig.5. From Fig. 5(b), we see that with increasing Γ, both the excited state density(β') and the excited state superfluidity($|\gamma'|$) decrease; they eventually vanishes for large Γ. In contrast, as shown in Fig. 5(a), the ground state density($|\psi|^2$) increases and hence the ground state superfluidity($|\psi|$) also increases with Γ. We note that this phenomenon can be understood as follows. Since a larger number of Rydberg excitation are destroyed for larger decay rate Γ, the ground state density of the atoms increase so that n_{total} may remain constant. In the deep superfluid limit, within the classical field approximation the ground state number density is same as the superfluid density $|\psi|^2$ neglecting the quantum fluctuations. However, in the correlated regime the superfluid density significantly deviates from the number density due to enhanced quantum fluctuations and ground state SF order parameter decreases with increasing Γ as seen in the hard core limit. To study quantum fluctuations in the ground state superfluidity, more careful analysis is required which is beyond the scope of the simple ansatz (Eq. 24) for the density matrix.

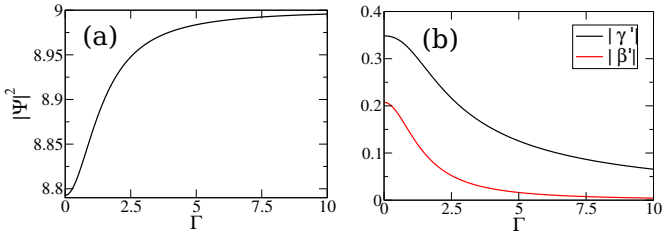

FIG. 5. (a) Plot of the steady state value of the ground state boson density $|\psi|^2$ with Γ showing the increase of ground state boson density with increasing Γ. (b) Plot of steady state values of $|\gamma'|$ and β' as a function of Γ. For both plots, $zV = 2$, $zJ = 1$, $\eta = \mu = 1$, $U = 0.6$ and $\Gamma = 0.2$. The total boson density is fixed at $n_{total} = 9.0$.

To obtain the dispersion of collective excitations in the deep SF phase, we calculate the fluctuation above the steady state values and decompose the fluctuation into Fourier modes similar to that for the hardcore boson case in the strong interacting regime. Also we choose the steady state value of γ' to be $\gamma_1 = \psi\gamma'/|\psi|$ so as to have a specific relative phase between ψ and γ', where $\psi_1 = |\psi|\exp[i\theta_\psi]$ is the steady state value of ψ and θ_ψ is the phase of ψ which is undetermined up to a global phase factor. An analogous calculation yields

$$\begin{aligned}
\lambda\delta\psi_{\vec{k}} &= i[J\epsilon(\vec{k})\delta\psi_{\vec{k}}/2 - 2U|\psi_1|^2\delta\psi_{\vec{k}} - U\psi_1^2\delta\psi^*_{\vec{k}} + \tilde{\mu}\delta\psi_{\vec{k}} \\
&\quad -\lambda_0 U\psi_1\delta\beta'_{\vec{k}} - \lambda_0 U\beta'\delta\psi_{\vec{k}} - \delta\gamma'^*_{\vec{k}}] \\
&\quad +\Gamma(\psi_1\delta\beta'_{\vec{k}} + \beta'\delta\psi_{\vec{k}})/2 \\
\lambda\delta\beta'_{\vec{k}} &= i[\eta J(\gamma_1^*\delta\gamma'_{\vec{k}} - \gamma_1\delta\gamma'^*_{\vec{k}})(z - \epsilon(k))/2 + (\psi_1^*\delta\gamma'^*_{\vec{k}} \\
&\quad +\gamma_1^*\delta\psi^*_{\vec{k}} - \psi_1\delta\gamma'_{\vec{k}} - \gamma_1\delta\psi_{\vec{k}})] - \Gamma(|\psi_1|^2\delta\beta'_{\vec{k}} \\
&\quad +\psi_1^*\beta'\delta\psi_{\vec{k}} + \psi_1\beta'\delta\psi^*_{\vec{k}}) \qquad (29) \\
\lambda\delta\gamma'_{\vec{k}} &= i[\eta z J\gamma_1\delta\beta'_{\vec{k}} + \eta J\epsilon(\vec{k})(\beta' - 1/2)\delta\gamma'_{\vec{k}} - \tilde{\mu}\delta\gamma'_{\vec{k}} \\
&\quad -2\psi_1^*\delta\beta'_{\vec{k}} - (2\beta' - 1)\delta\psi^*_{\vec{k}} + V\gamma_1\epsilon(\vec{k})\delta\beta'_{\vec{k}}/2 \\
&\quad +zV\beta'\delta\gamma'_{\vec{k}}/2 + \lambda_0 U(\psi_1^*\gamma_1\delta\psi_{\vec{k}} + \psi_1\gamma_1\delta\psi^*_{\vec{k}} + |\psi_1|^2 \\
&\quad \times\delta\gamma'_{\vec{k}})] - \Gamma(|\psi_1|^2\delta\gamma'_{\vec{k}} + \psi_1^*\gamma_1\delta\psi_{\vec{k}} + \psi_1\gamma_1\delta\psi^*_{\vec{k}})/2
\end{aligned}$$

where $\tilde{\mu} = \mu - E'_f$ is the modified chemical potential, E'_f is the frequency of oscillation of ψ and γ', λ is the complex eigenvalue, $\epsilon(\vec{k}) = 2\sum_{i=1..d}\cos k_i$, d is the dimension and $\delta\psi_{\vec{k}}$ and $\delta\gamma'_{\vec{k}}$ are the fluctuations of ψ_1 and γ_1 respectively. These three equations are supported with another two equations of $\delta\psi^*_{\vec{k}}$ and $\delta\gamma'^*_{\vec{k}}$. From the resulting 5×5 matrix we numerically find out the five eigenvalues out of which one is real with $\lambda_R < 0$ and other four complex eigenvalues come with pair(complex conjugate to each other). Out of these two pairs of complex eigenmodes, imaginary part of one gives gapless sound mode [see Fig.6(a)] at $\vec{k} = 0$ while the other provides the gapped collective mode [see Fig. 6(b)]. The linear dispersion (sound mode) can be seen from Fig.6(a) and its slope yields the sound velocity v_s. Similar to the superfluid density v_s also increases with Γ.

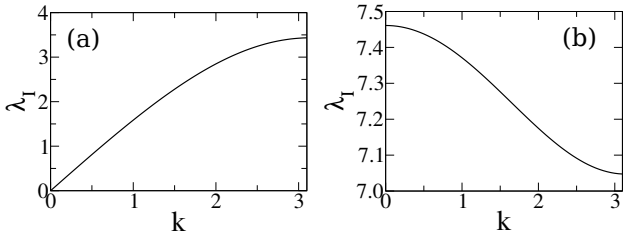

FIG. 6. (a)Plot of the dispersion of the gapless sound mode as a function of k (for diagonal cut in the Brillouin zone) in the deep SF phase. (b) Plot of the highest gapped eigenmode as a function of k. For both plots $\Gamma = 0.2$. All parameters are same as in Fig. 5

V. NON-EQUILIBRIUM DYNAMICS FOR HARDCORE BOSONS

In this section, we study the effect of linear ramp in Γ and J. To this end, we construct the initial density matrix of the system from the steady states obtained in the SF phase for a given Γ_i and J_i and linearly vary either Γ or J through its critical value. This is done, for example, by choosing $J(t)$ to be

$$J(t) = J_i + (J_f - J_i)t/t_{\max} \qquad (30)$$

where $J_{f(i)}$ is the final(initial) value of the hopping matrix element J which corresponds to a steady state belonging to the MI(SF) and $t_{\max}$ is the ramp time. A similar protocol is chosen for variation of Γ keeping J fixed. In what follows, we concentrate on the change in the superfluid order parameters(α, β) as a function of time following and the change in the entropy(S) across the dynamical transition. To do this, we numerically solve the density matrix equation,

$$\frac{\partial\hat{\rho}_i}{\partial t} = -i\left[\hat{H}_i^{MF}[J(t)], \hat{\rho}_i\right] + \hat{\mathcal{L}}\hat{\rho} \qquad (31)$$

which corresponds to variation of J with fixed Γ. An analogous equation can be easily written for the case when Γ is varied keeping J fixed.

A typical behavior of superfluid order parameters $|\alpha|, |\beta|$ and entropy S as a function of time is shown in Fig. 7 for $t_{\max} = 500$ (in units of $1/\Omega$). We find that when Γ is varied keeping J fixed, $S(t)$ monotonically increases and peaks when the system crosses the phase boundary (Fig. 7(b)). Upon entering the MI phase, S decreases monotonically till $t = t_{\max}$. In contrast, when J is varied keeping Γ fixed, the entropy S monotonically increases in the SF phase and finally saturates in the MI phase(Fig. 7(d)). The behavior of S for the former protocol originates from an enhanced rate of destruction of Rydberg

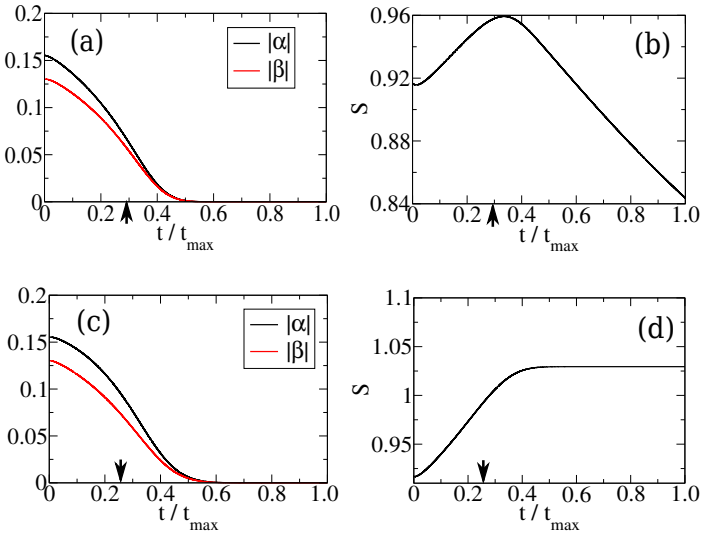

FIG. 7. (a) Plot of superfluid order parameter amplitudes $|\alpha(t)|$ and $|\beta(t)|$ as a function of t during a linear ramp of Γ (with $\Gamma_i = 0.8$ to $\Gamma_f = 2.5$ and $zJ = 8$) from the SF to the MI phase. The critical point is reached at $t = 0.4t_{\rm max}$ as marked in the figure. All other parameters are same as in Fig. 1(b). (b) Similar plot for the entropy S. All parameters are same as in (a). (c) and (d) Similar plots as (a) and (b) respectively but during linear ramp of J ($zJ_i = 8$ to $zJ_f = 2$) with fixed $\Gamma = 0.8$. All other parameters are same as in (a). The arrows indicate the time at which the critical point is crossed during the dynamics. Note that S shows qualitatively distinct behavior for the two protocols.

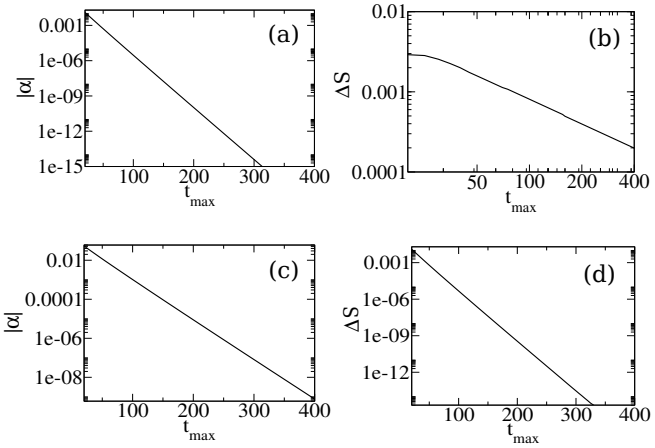

FIG. 8. (a) Plot of $|\alpha|$ and ΔS evaluated at $t = t_{\rm max}$ (at the end of the ramp) as a function of $t_{\rm max}$ for linear ramp of Γ ($\Gamma_i = 0.8$ $\Gamma_f = 2.5$ for $zJ = 8$) are shown in log scale. $|\alpha|$ shows exponential fall whereas ΔS shows power law fall with $t_{\rm max}$. (c)-(d) Both $|\alpha|$ and ΔS shows exponential fall with $t_{\rm max}$ while ramp in J from $zJ_i = 8$ to $zJ_f = 2$ for $\Gamma = 0.8$.

excitations as Γ is increased; this leads to larger weight of the system in the ground state and thus to vanishing S. In contrast, for the second protocol where Γ is held fixed, the rate of decay of excitations is held constant; the dynamics merely cease to produce new excitations due to a large Mott gap in the low-energy sector. In addition, the fixed rate of Γ ensures that the system reaches a steady state. This leads to decay of S in the MI phase for the first protocol and its constant value for the second. The difference between the behavior of S for the two protocols mentioned above can also be understood by noting that in Eq. 7, the dynamics due to the quench of the hopping term J is generated only through its direct coupling with the SF order parameters which decays exponentially with time in the insulating phase; hence the effect of J vanishes in the long time dynamics. On the other hand the dissipation term Γ is coupled to the occupation number and other parameters which in turn gives rise to non-trivial asymptotic behavior of S for the linear quench of Γ.

For both the cases the entropy generation rate shows a distinct change near the phase boundary. Also, $|\alpha|$ and $|\beta|$ monotonically decrease as one moves from the SF to the MI phase [Fig.7(a) and (c)]. This can be understood as a characteristic of evolution of a system with finite dissipative parameter which suppresses quantum oscillations of these quantities; we note that this constitutes an essential qualitative difference between time evolution of Rydberg atoms and other ultracold bosons system where dissipation is absent.

Next, we study the deviation of entropy, $\Delta S = |S(t_{\rm max}) - S_0|$ from the final steady state value S_0 and the SF order parameter amplitude $|\alpha(t_{\rm max})| \equiv |\alpha|$ as a function of $t_{\rm max}$ for both the protocols. The variation $|\alpha|$ and $\Delta S(t_{\rm max})$ is shown in Figs. 8(a) and (b) for a ramp of Γ and in Figs. 8(c) and (d) for a ramp of J. For both the protocols with linear ramp the SF order parameter amplitude $|\alpha|$ decays exponentially with the ramp rate $t_{\rm max}$ which is evident from the linear fall of $|\alpha|$ when plotted in log-scale, as shown in Fig.8(a) and (c). In contrast, ΔS behaves differently for two types of linear ramping protocols. For a ramp of Γ with fixed J, we find that ΔS decays as a power law $\sim 1/t_{\rm max}^{\kappa}$. In Fig.8(b), we plot ΔS as a function of $t_{\rm max}$ in log-log scale and obtain the value of the exponent $\kappa \simeq 1.0$ from the slope of the linear portion of the curve. In contrast for a ramp of J with fixed Γ, ΔS falls off exponentially with quench rate $t_{\rm max}$ as shown in Fig.8(d).

We note in this context that the behavior of defect density or equivalently entropy as a function of ramp rate through a critical point has been studied in several context both for closed[22,23] and open[24,25] quantum systems. The latter class of system features dissipation and noise via coupling to an external bath; this leads to a scaling of defect density $n \sim \gamma(k_B T)^3/v_0$, where T is the temperature of the external bath, γ is the coefficient of dissipation, and v_0 is the ramp rate. However, it is to be noted that such a scaling is derived with the assumption that

the system reaches an adiabatic regime after crossing the critical point and that γ remains constant through the drive; in this case, no defect is produced or annihilated when the system reaches the adiabatic regime for which $\gamma, T \ll \Delta_0$, where Δ_0 is the instantaneous energy gap. In contrast, for a ramp of Γ for the Rydberg atoms studied here, the system does not reach an adiabatic regime in the MI phase once it crosses the critical point. Thus the scaling arguments of Refs. 24 and 25 can not be directly used for explaining the scaling behavior of ΔS that we obtain here; an appropriate analysis of this phenomenon is beyond the scope of the present study.

VI. DISCUSSION

In this work, we have studied non-equilibrium phases, collective modes and quench dynamics of Rydberg atoms in an optical lattice. We note that the spontaneous decay of Rydberg excited states implies that a collection of Rydberg atoms constitute a non-equilibrium quantum many body system whose dissipation may be modeled by a decay rate Γ. In this work, we have analyzed such non-equilibrium systems within the framework of Lindbald master equation describing the time evolution of the density matrix within mean-field theory.

In the first part of this work, we have considered the Rydberg atoms in the limit of on-site repulsion between the atoms and obtained the fixed points of their density matrix equations corresponding to both the SF and MI steady states. In contrast to the usual MI phases of ultracold atoms systems, we find that the present system allows for insulating phases that can have incommensurate filling. We analyze the fixed points and find that MI-SF transition in these systems are continuous which may be inferred from the discontinuous jump of $dS/d\Gamma$ at the transition. We have also numerically studied the steady states of the Rydberg atoms with finite on-site repulsion by constructing the initial density matrix from the Gutzwillers wavefunction. We find that the transition in such systems are qualitatively similar to the one for atoms with infinite on-site repulsion. This justifies our analysis for the hard core bosons from the point of view of possible experiments on the system.

We have also looked into the collective modes of such systems by carrying out a linear stability analysis of the MI and SF fixed points. The real part of the corresponding eigenvalues indicates stability of the corresponding phases, whereas the imaginary part give collective excitation frequencies. Such an analysis yields both gapless sound mode and gapped collective modes in the superfluid phase; in contrast, all modes in the insulating phase are gapped. The velocity of the sound mode vanishes at the phase boundary; also the energy gap increases linearly in the insulating phase near the transition point. This allows us to infer $z = 2$ and $\nu = 1/2$ for the MI-SF transition within mean-field theory.

We have analyzed the Rydberg system in the deep SF limit for weak U by using a coherent state representation of the system density matrix. Our analysis results in a dynamical equation of the condensate in this limit; this equations is the counterpart of the Gross-Pitaevskii equation for dissipative systems. We analyze this equation to find that in the classical regime where the boson fluctuations can be ignored, both the ground state density and the superfluid order parameter amplitude increases with increasing dissipation strength. This, somewhat counterintuitive, result originates from the fact that the total system density is a constant of motion in this regime; thus a large Γ which leads to larger loss of Rydberg excitations automatically leads to a larger ground state density. We also obtain the gapless sound mode and the gapped collective modes by a stability analysis of the density matrix equations around the SF fixed point in this regime.

Finally we investigated the non-equilibrium dynamics for a linear ramp of either J or Γ which takes the system from the SF to the MI phase. Unlike systems without dissipation, for linear ramp, the superfluid order parameters do not show any oscillations and decay monotonically in the insulating phase due to the presence of dissipation for both the protocols. In contrast, we find that the behavior of the entropy S as a function of time during the linear ramp is qualitatively different for a ramp of Γ with fixed J and for a ramp of J with fixed Γ; for the former protocol, S decreases with time while it remains constant for the latter protocol once the system enters the MI phase. However, in both cases S changes slope near the phase boundary. We also investigate in the long time dynamics the deviation of the entropy from its steady state value, which shows exponential decrease with ramping rate for the linear quench of J. In contrast, $\Delta S \sim 1/t_{\rm max}$ for the quench of Γ. Such a power law arises out of the reduction of the density of Rydberg excitation of the system with increasing Γ; its detailed analysis is left for a possible future project.

Several recent experiments has been carried out for systems of Rydberg atoms[26–28]. The easiest experimental verification of our result would constitute performing boson momentum distribution measurement for a system of Rydberg atoms in a 3D optical lattice. Such measurement would detect the emergence of a central peak in the momentum distribution, as measured in a standard time of flight experiment[29], as one enters the SF phase. Thus such measurements may be used to chart out the MI-SF phase boundary in the $J - \Gamma$ plane. The corresponding collective modes can also be measured by standard lattice modulation, RF, or Bragg spectroscopy in these systems[30].

In conclusion, we have studied a system of Rydberg atoms in the presence of dissipation using a density matrix formulation within mean-field theory. Our work constitutes an analysis of these dissipative atom system which may take into account their SF phases by going beyond the frozen atom limit; it may thus serve as the first step towards a more complete picture of the description of the phases and dynamics of these atoms beyond

mean-field theory where the effects associated with quantum fluctuations are treated more rigorously. We have charted out the MI-SF phase-boundary of such a system and derived expressions for the collective modes in each of the phases. We have also studied non-equilibrium dynamics of these systems for linear ramp protocol of both J and Γ and identified a $1/t_{\rm max}$ scaling of ΔS for ramp of Γ. We have suggested experiments which may test our theory.

[1] M.D. Lukin, M. Fleischhauer, and R. Cote *et al.*, Phys. Rev. Lett.**87**, 037901 (2001); D. Jaksch, J. I. Cirac, and P. Zoller, S. L. Rolston, R. Cote and M. D. Lukin, Phys. Rev. Lett.**85** 2208 (2000).

[2] R. Heidemann, U. Raitzsch, V. Bendkowsky, B. Butscher, R. Lw, L. Santos and T. Pfau, Phys. Rev. Lett. **99**, 163601 (2007); E. Urban, T. A. Johnson, T. Henage, L. Isenhower, D. D. Yavuz, T. G. Walker, and M. Saffman, Nat. Phys. **5**, 110 (2009); A. Gaitan, Y. Miroshnychenko, T. Wilk, A. Chotia, M. Viteau, D. Comparat, P. Pillet, A. Browaeys, and P. Grangier, Nat. Phys. **5**, 115 (2009).

[3] F. Cinti, P. Jain, M. Boninsegni, A. Micheli, P. Zoller, and G. Pupillo , Phys. Rev. Lett. **105**, 135301 (2010).

[4] R Mukherjee, J Millen, R Nath, M P A Jones and T Pohl, J. Phys. B:At. Mol. Opt. Phys. **44** 184010 (2011); A. W. Glaetzle, M. Dalmonte, R. Nath, I. Rousochatzakis, R. Moessner, and P. Zoller, Phys. Rev. X **4**, 041037 (2014).

[5] N. Henkel, R. Nath and T. Pohl, Phys. Rev. Lett.**104**, 195302 (2010); J. Honer, H. Weimer, T. Pfau, and H. P. Büchler, Phys. Rev. Lett. **105**, 160404 (2010).

[6] R. Low, H. Weimer, U. Krohn, R. Heidemann, V. Bendkowsky, B. Butscher , H. P. Büchler, and T. Pfau, Phys. Rev. A **80**, 033422 (2009); H. Weimer, R. Low, T. Pfau, H. P. Büchler, Phys. Rev. Lett. **101**, 250601 (2008).

[7] H. Weimer, M. Moller, I. Lesanovsky, P. Zoller, and H. P. Büchler, Nat. Phys., **6**, 382(2010); H. Weimer, M. Muller, H.P. Büchler, and I. Lesanovsky, Quant. Inf. Proc. **10**, 885 (2011).

[8] T. Pohl, E. Demler, and M.D. Lukin, Phys. Rev. Lett.**104**, 043002 (2010); H. Weimer and H. P. Büchler, Phys. Rev. Lett. **105**, 230403 (2010).

[9] I. Leasanovsky and H. Katsura, Phys. Rev. A**86**, 041601 (2012); I Leasonvsky, Phys. Rev. Lett.**106**, 025301 (2011).

[10] B. Olmos, R. Gongalez-Ferez, and I. Lesanovsky, Phys. Rev. Lett.**103** 185302 (2009).

[11] B. Vaucher, S.J. Thwaite, and D. Jaksch, Phys. Rev. A **78**, 043415 (2008).

[12] S. Ji, C. Ates, and I. Lesanovsky, Phys. Rev. Lett.**107**, 058223 (2001).

[13] M. Viteau, M. G. Bason, J. Radogostowicz, N. Malossi, D. Ciampini, O. Morsch, and E. Arimondo, Phys. Rev. Lett.**107**, 060402 (2011).

[14] K. Saha, S. Sinha, and K. Sengupta, Phys. Rev. A**89**, 023618 (2014).

[15] R. Löw *et al.*, J. Phys. B **45**, 113001 (2012).

[16] C. Carr, R. Ritter, C. Wade, C. S. Adams, K. J. Weatherill, Phys. Rev. Lett.**111**, 113901 (2013).

[17] M. Marcuzzi, E. Levi, S. Diehl, J. P. Garrahan, and I. Lesanovsky, Phys. Rev. Lett.**113**, 210401 (2014).

[18] T. E. Lee, H. Haffner and M. C. Cross, Phys. Rev. A**84**, 031402(R) (2011).

[19] I. Lesanovsky, J. P. Garrahan, Phys. Rev. Lett.**111**, 215305 (2013); Phys. Rev. A**90**, 011603 (2014).

[20] A. Hu, T. E. Lee, and C. W. Clark, Phys. Rev. A**88**, 053627(2013).

[21] E. C. G. Sudarshan, Phys. Rev. Lett.**10**, 277 (1963); R. J. Glauber, Phys. Rev. **131**, 2766 (1963).

[22] T. W. B. Kibble, Phys. Rep. **67**, 183 (1980); W. H. Zurek, Phys. Rep. **276**, 177(1996).

[23] J. Dziarmaga, Adv. Phys. **59**, 1063 (2010); A. Polkovnikov, K. Sengupta, A. Silva, and M. Vengalattore, Rev. Mod. Phys. **83**, 863 (2011).

[24] P. Nalbach, S. Vishveshwara, and A. A. Clerk, Phys. Rev. B**92**, 014306 (2015)

[25] D. Patane, A. Silva, L. Amico, R. Fazio, and G. E. Santoro, Phys. Rev. Lett.**101**, 175701 (2008).

[26] A. Urvoy, F. Ripka, I. Lesanovsky, D. Booth, J. P. Shaffer, T. Pfau and R. Low, Phys. Rev. Lett. **114**, 203002 (2015).

[27] N. Malossi, M. M. Valado, S. Scotto, P. Huillery, P. Pillet, D. Ciampini, E. Arimondo, and O. Morsch, Phys. Rev. Lett. **113**, 023006 (2014); R. Faoro, C. Simonelli, M. Archimi, G. Masella, M. M. Valado, E. Arimondo, R. Mannella, D. Ciampini, O. Morsch, arXiv:1506.08463 (unpublished).

[28] D. Barredo, H. Labuhn, S. Ravets, T. Lahaye, A. Browaeys and C. S. Adams, Phys. Rev. Lett. **114**, 113002 (2015); D. Paredes-Barato and C. S. Adams, Phys. Rev. Lett. **112**, 040501 (2014).

[29] I. Bloch, J. Dalibard, and W. Zwerger, Rev. Mod. Phys. **80**, 885 (2008).

[30] S. Gupta, Z. Hadzibabic, M.W. Zwierlein, C.A. Stan, K. Dieckmann, C.H. Schunck, E.G.M. van Kempen, B.J. Verhaar, and W. Ketterle, Science **300**, 1723 (2003); J. T. Stewart, J. P. Gaebler and D. S. Jin, Nature **454**,744 (2008); U. Bissbort, S. Gtze, Y. Li, J. Heinze, J. S. Krauser, M. Weinberg, C. Becker, K. Sengstock, W. Hofstetter, Phys. Rev. Lett. **106**, 205303 (2011); R. Sensarma, K. Sengupta, and S. Dassarma, Phys. Rev. B **84**, 081101 (R) (2011); R. Sensarma, D. Pekker, M. D. Lukin, and E. Demler Phys. Rev. Lett. **103**, 035303 (2009).